Ion bombardment effects on nucleation of sputtered Mo nano-crystals in Mo/B4C/Si multilayers

Patelli, A.; Rigato, V.; Salmaso, G.; Carvalho, N. J. M.; De Hosson, J. Th. M.; Bontempi, E.; Depero, L. E.

Published in:
Surface & Coatings Technology

DOI:
10.1016/j.surfcoat.2005.11.072

Available online at www.sciencedirect.com
SCIENCE DIRECT®
Surface & Coatings Technology 201 (2006) 143 – 147
SURFACE & COATINGS TECHNOLOGY
www.elsevier.com/locate/surfcoat

Ion bombardment effects on nucleation of sputtered Mo nano-crystals in Mo/B4C/Si multilayers

A. Patelli [a,*], V. Rigato [a], G. Salmaso [a], N.J.M. Carvalho [b], J.Th.M. De Hosson [b], E. Bontempi [c], L.E. Depero [c]

[a] LNL-INFN, Via dell'Università 2, 35020 Legnaro, Padova, Italy
[b] Department of Applied Physics, University of Groningen, Nijenborgh 4-9747 AG Groningen, The Netherlands
[c] INSTM, Laboratorio di Chimica per le Tecnologie, Università di Brescia, 25123 Brescia, Italy

Received 11 March 2005; accepted in revised form 7 November 2005
Available online 13 December 2005

Abstract

Over recent years, the introduction of Mo/Si multilayers mirrors with different barrier layers for the interfaces has allowed increasing mirror reflectance, life and temperature stability. The effects of these very thin barrier layers on multilayer growth, such as interlayer formation and Mo crystallization, are not completely understood and deserve further study. This work shows, by using XRD and TEM analysis, that the crystallization thickness of the sputtered deposited Mo layers, when the boron carbide interlayer is present, increases from 2.0 nm to about 2.6 nm with respect to conventional Mo/Si multilayers. Furthermore some effects of ion energy bombardment on the nano-crystals formation and interlayer structure evolution have also been studied, showing an increase of preferential orientation for higher ion energies.

PACS: 68.65.Ac; 61.43.-j; 68.55.Ac; 68.55.Jk
Keywords: Molybdenum; Silicon; EUV multilayer mirrors; Nucleation; Crystal microstructure

1. Introduction

Mo/Si-based multilayers have become essential for applications that require an optical system in the soft X-ray and EUV radiation range, such as those involving solar corona and disk observation [1] or the new generation lithography [2]. In such multilayers the period is just few nanometres and interfaces play a crucial role in the final mirror performance, as they must be sharp and smooth on the atomic scale in order to maximize reflectivity. In recent years, to increase the sharpness of these interfaces, C [3], Mo_2C [4] or B_4C [5] ultra thin barrier layers have been introduced in the Mo/Si systems. As expected, all these barrier layers have increased the thermal stability of the multilayer, however, only the introduction of boron carbide leads also to a reflectance increase up to 71% for normal incidence radiation at about 13 nm of wavelength, as forecast by the ideal structure simulations [6].

These findings encourage further studies into the Mo/Si multilayer systems with thin boron carbide interlayers, in order to investigate the interface formation and increase mirror reflectivity and stability. In particular, the Mo crystalline structure plays a key role in the multilayer performance and optimization. In fact, the main contribution in high and medium frequency mirror roughness is due to Mo grain nucleation and its lateral dimension [7]. Furthermore, it is a known fact that amorphous layers are sometimes useful for their lower roughness and intrinsic stress. For these reasons, for example, some tests have been performed on the introduction of Ru in Mo layers in order to inhibit nano-crystals growth [8]. Also the introduction of the boron carbide thin interlayer, of just 0.5 nm thick, seems to decrease the crystal size relative to the Mo/Si multilayers, leading to amorphous Mo layers [6]. On the other hand, the presence of the poly-crystalline Mo can increase system lifetime and thermal stability, because the nano-crystals (usually Mo(110) preferentially oriented in sputtering deposited multilayers) can hinder the diffusion of silicon atoms. Correlated to this blocking action is the reduced thickness of

* Corresponding author. Tel.: +39 049 8068 406; fax: +39 049 641 925.
E-mail address: alessandro.patelli@lnl.infn.it (A. Patelli).

0257-8972/$ - see front matter © 2005 Elsevier B.V. All rights reserved.
doi:10.1016/j.surfcoat.2005.11.072

the Si-on-Mo interface in Mo/Si multilayers with respect to the Mo-on-Si interface for example, and this asymmetry is also maintained in heat-treated samples [7]. The presence of Mo crystals is also beneficial to the optical properties because of its higher density, which assures the maximum optical contrast between the spacer and absorber layers.

In the case of conventional Mo/Si multilayers grown by sputtering, the mechanism of Mo grain nucleation has already been studied [9]. Mo layers are amorphous for thicknesses up to 2.0 nm, then a transition takes place from an amorphous to a poly-crystalline Mo structure and the nucleation thickness threshold seems to be as sharp as 0.2 nm. With Mo layer thickness less than 2.0 nm, nucleation is supposed to be hindered by the presence of Si atoms in concentrations higher than the solubility limit in the Mo crystal.

In this work we have investigated the Mo grain nucleation threshold for Mo/Si multilayers produced by RF-magnetron sputtering with a few angstroms thick boron carbide interlayers on both interfaces. The knowledge of the growth conditions is essential to understand the process, therefore the energy of different particles impinging onto the surface has been estimated by calculations and experimental measurements. In particular the amorphous-to-crystal transition was investigated for two different bombarding argon ion energies, in order to highlight the effects of the low energy ion assistance during growth and to optimise further the deposition process.

2. Experimental

The experimental apparatus used at LNL for producing the X-ray/EUV mirrors is similar to that described in a previous paper [10]. It consists of three planar 2 in. UHV type II unbalanced magnetron sputter sources in an upward configuration and a three-position bias able sample holder. The distance between Mo and Si targets and substrate is set at 16.5 cm, while for the B_4C target it is set at 10 cm, this geometry guarantees a film uniformity of better than 1% over an area 2×2 cm^2. Deposition is static and Ar (99.9999%) was used as process gas at an operating pressure of $3.3\cdot10^{-3}$ mbar. The base pressure in the chamber is about $5.0\cdot10^{-7}$ mbar. Each source is driven by an RF power supply at 13.56 MHz, with 60 W power for Mo, 150 W for Si and 200 W for B_4C. The effective deposition rates for all the sources are about $2.7\cdot10^{14}$ At/cm^2 s. In order to monitor the deposition rates, the system is equipped with 2 quartz microbalances. Samples can be biased with the aid of a power amplifier at bias voltages (V_B) ranging from −100 V to +100 V. Ion density, electron temperature and plasma potential (V_p) measurements were carried out by a cylindrical Langmuir probe suited for RF plasma diagnostics (Scientific Systems SmartProbe™). The measurements were taken for the different substrate biases applied at about 1 cm from the sample surface.

The X-ray microdiffraction (μXRD) spectra were collected using a D/max-RAPID Rigaku microdiffractometer, equipped with a cylindrical 2D imaging plate (IP) detector from −45° to 160° (2θ). For these experiments, the irradiated area was 300 μm^2 and the incident grazing angle was 5°.

The RBS and NRA measurements were performed using the HVEC 2.5 MV and CN 7.0 MV Van de Graaff accelerators at the LNL - INFN. A 2.2 MeV α-beam at a scattering angle of 170° was used for characterizing the Mo, Ar and Si content. Furthermore, stoichiometry and absolute areal densities of B and C were obtained by α-1.85 MeV RBS analysis at a scattering angle of 165° where both are essentially Rutherford [11,12] and by nuclear reaction analysis, using $^{11}B(p,\alpha)^8Be$ [13], $^{11}B(d,\alpha_0)^9Be$ and $^{12}C(d,p)^{13}C$ reactions.

A transmission electron microscopy (TEM) was used to study the microstructure of the as-deposited multilayers. The analyses were performed using the microscopes JEOL 4000 EX/II operating at 400 kV and JEOL 2010 FEG operating at 200 kV, both located at the University of Groningen. Cross-sectional TEM specimens were prepared using a method described in detail elsewhere [14].

3. Results

Since the substrate temperature is about 40 °C during the sputtering deposition process the main energy contribution to growth is due to atoms, ions and reflected neutrals impinging onto the surface.

In order to evaluate the energy of the Mo atoms, the mean energy of the sputtered atoms was calculated by TRIM.SP simulation code. The krypton-carbon potential [15] was chosen as the ion-target interaction potential [16] and for the inelastic loss a +50%–50% contribution of non-local loss due to Lindhard [17] and a local loss due to Oen–Robinson [18] were applied. The surface binding energy for Mo was set at 6.83 eV and the weighted average of isotopes' natural abundance was taken for the atomic masses. The incident energy of ions was supposed to be monochromatic considering the DC self-bias potential of the cathode (−300 V) as accelerating potential. The mean energy of sputtered atoms along the normal of the target was about 13.0 eV. The energy loss due to the thermalisation effect during transport from the target to the substrate was evaluated using the simplified Drüsedeau model [19], which divides the sputtered atom into a ballistic and a diffused population.

In order to estimate the characteristic pressure-distance product (pd), the deposition rate was recorded as a function of the pd product using the quartz microbalances calibrated by RBS measurements. The characteristic value and the ballistic and diffused population of the sputtered atoms can be obtained by fitting the results. In order to roughly quantify the mean energy of the adatoms we can assume that, since gas thermal energy is only a few hundredths of an eV, the ballistic atoms transport nearly all the energy. As a first approximation, therefore, the energy deposited on the substrate can be obtained by the product of the mean energy to the fraction of the ballistic flux. Using this approach the mean Mo adatoms energy results about 9.7 eV.

Also, due to the higher Mo mass with respect to Ar, during the sputter deposition of the Mo layers the substrate is bombarded by Ar ions reflected and neutralised on the target surface. The TRIM.SP [20] simulations were used to evaluate

this contribution as well. The calculations give a reflection coefficient R_N of about 0.24, therefore their contribution cannot be neglected. In order to quantify the flux and energy of the bombardment at the substrates, the angular and energy distributions were integrated using the measured value of Ar^+ cathode current. The average energy at the substrate of backscattered Ar is about 39.3 eV taking into account the thermalisation effects [21], with a ratio between reflected neutrals and adatoms of about 0.5.

The last energy contribution to film growth is expected by ions impinging the surface. Plasma diagnostics were performed to estimate their flux and energy. The plasma potential (Vp) is 24±1 V and the electron temperature about 4.3 eV. Ion density is about $2.0 \cdot 10^9$ ions/cm^3 corresponding to an ion to atoms flux ratio of about 2. The energy contribution of Ar ions can be easily controlled by applying a DC-bias to the substrate (Vb). The resulting ion energy is the difference (Vp − Vb), because sample-holder biases lower than floating potential do not influence plasma potential. The effect of ion bombardment during growth depends strongly on the ion energy. As a matter of fact, energy transfer to the adatoms is performed by collisions that can allow either surface or bulk displacement of the atoms. The displacement process is characterized by a threshold energy depending on the bonds of the atoms in the film and, as the coordination numbers of the atoms on the surface and in the bulk are different, two different threshold energies can be determined for the surface and bulk displacement. The surface displacement energy threshold is usually assumed as one half of the threshold in the bulk. Ma and Kido [22] have achieved an analytical solution for the impinging ion damage energy relative to the atomic displacement on the surface and in the bulk. The results of the deposited energy per incident Ar ion that causes atoms displacement are shown for Mo and Si in Fig. 1. The displacement energy was set for Mo at 33 eV and for Si at 13 eV [20]. We can see that there is an energy window for both

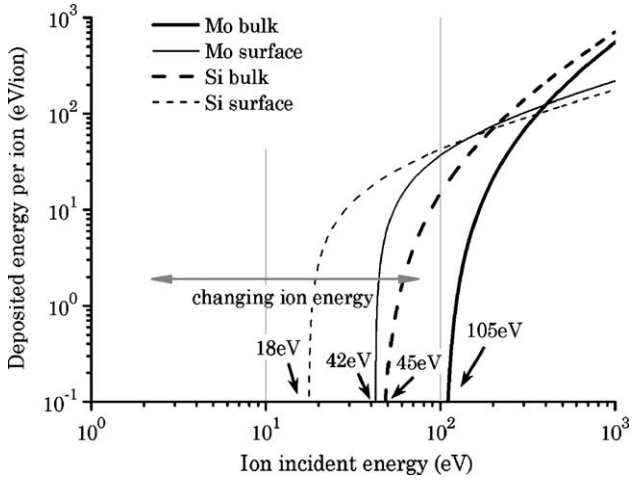

Fig. 1. Calculated energy deposited in displacement of Mo and Si atoms by Ar ions in Mo and Si growing thick films on the surface and in the bulk as a function of Ar ion incident energy [23]. In the figure the threshold energies for surface and bulk displacement are indicated. The presence of an ion energy window that allows surface but not bulk displacement of the adatoms can be observed.

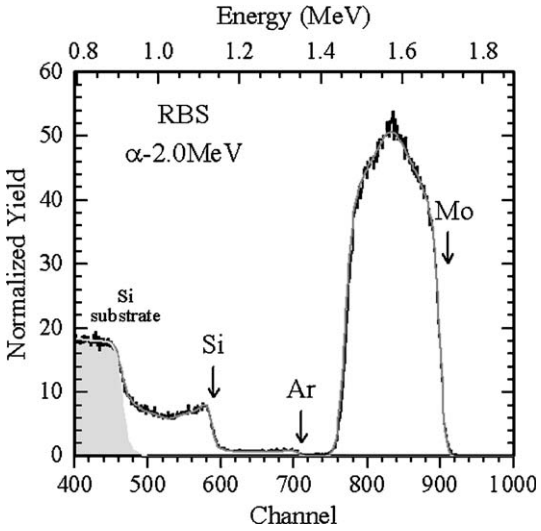

Fig. 2. α-2.0M eV RBS spectrum and simulation of the depth graded multilayer sample produced at the ion energy bombardment of 24 eV.

elements where the allowed atom displacement is concentrated on the surface. Therefore in order to study the effect of the ions on the grain nucleation, attention was focused on ion bombardment energies of 24 eV and 74 eV, with one below the Mo energy window and the other in the middle.

In order to investigate Mo grain nucleation by TEM analysis in cross section, two Mo/B_4C/Si/B_4C multilayer samples were produced at the two different bombarding ion energies with graded Mo layer thickness. Mo layer thickness ranges from 1.7 to 3.5 nm in steps of 0.3 nm. Each layer thickness is repeated three times in order to increase the statistics of the TEM information. Furthermore, to study possible stress/thickness effects on growth, the structure was grown starting from the thinner layers close to the substrate and then, once the thickest layer had deposited, the structure was repeated and inverted with the thinnest layer close to the top. The structure of the multilayers was controlled by RBS and nuclear reaction analysis. Fig. 2 shows the RBS spectrum and the simulation of one of the two multilayers. By RBS and NRA measurements, assuming bulk densities, Si layers are about 50 Å thick and the B_4C ones about 4 Å. Ar content in the Si layers is about 5 at.%, while no argon can be detected in Mo layers [23]. The Ar content is supposed to be uniformly diluted in the spacer layer without creating bubbles, which were not observed by HRTEM. Oxygen and nitrogen contamination in the film are lower than the detection limit of 1 at.%. The boron carbide stoichiometry was measured in the multilayers and in thick films. The B-to-C concentration ratio was 4.4±0.3, similar ratios can be found in literature relative to the growing conditions [24].

Fig. 3 shows the bright and dark field TEM images of a portion of the cross-section view. The bright field image is useful to observe both the multilayer and the interfaces structure. The silicon layers appear with a brighter colour in the bright field, while Mo layers appear darker due to the higher atomic density. On the other side the dark field images are obtained by selecting the objective aperture of the single diffracted beam of the Mo(110) reflection. In this way only the

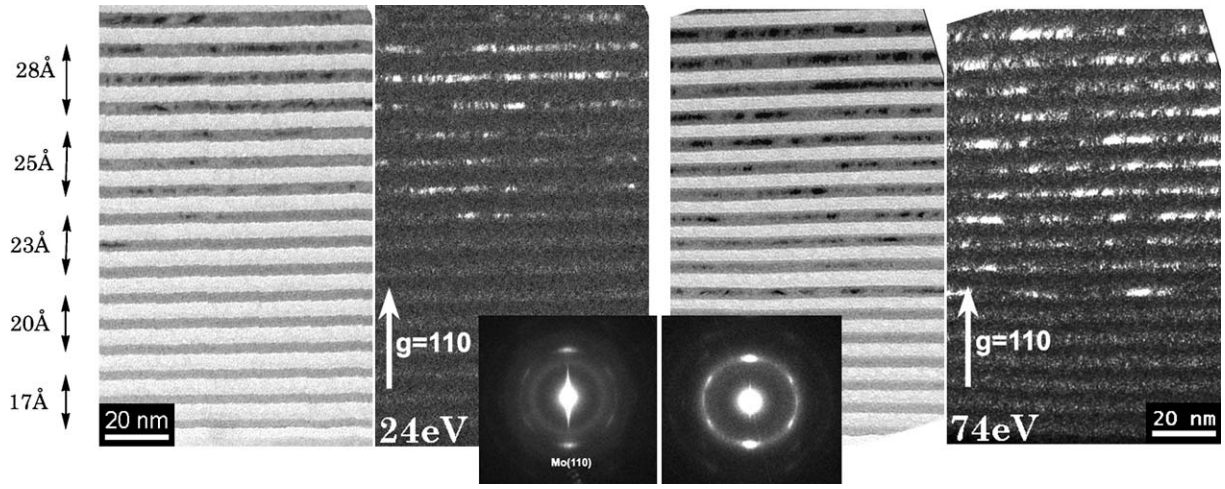

Fig. 3. Bright and dark field cross-sectional HRTEM images of the depth graded multilayers grown at 24 eV (left) and 74 eV (right) Ar^+ energy bombardment. On the left side the single Mo layer thickness is indicated: the indicated thickness is the same for groups of three layers. In the centre it is shown as an example an electron diffraction pattern.

Mo grains that are preferentially oriented with the Mo(110) direction parallel to growth direction are highlighted in white. In fact, with the electron diffraction pattern, which is also shown in Fig. 3 (central insert), the growth direction can be determined by the in-line spots close to zero order diffraction, due to the multilayer structure and the spot due to the Mo(110) reflection appears also in the same direction.

A higher magnification study of the layers and of their interfaces (not reported in this paper) shows that the multilayers are characterized by sharp and smooth interfaces for both the amorphous and the crystalline layers. The interlayer thickness is within the atomic scale range. As a first finding, Fig. 4 shows that the Mo layers with thickness of 1.7 and 2.0 nm are amorphous for both bombarding ion energies. On the contrary, for both bombarding energies, the 2.8, 3.2 and 3.5 nm thick layers clearly show the presence Mo nano-crystals. It is interesting to observe that the Mo grain size in the growth direction appears to be the same thickness as the Mo layer. A difference between the two ion energies can be found in the orientation of these grains. In fact, in the dark field images the sample submitted to higher energy bombardment shows a denser white area, which suggests a decrease of the angular spread of Mo(110) grains along the growth direction. This finding is not due to an instrumental measurement effect because it is also confirmed by the micro-diffraction analysis already presented in [25] and it can be attributed to the induced higher surface adatoms mobility, as predicted by calculation (see Fig. 1). Furthermore we can see that the ion energy of 74 eV is in the energy window allows surface but not bulk mobility. We can also see from the TEM data a great increase in the interface thickness, even in the Mo-on-Si interface whereas usually the Mo/Si multilayers are more affected by the mixing effect.

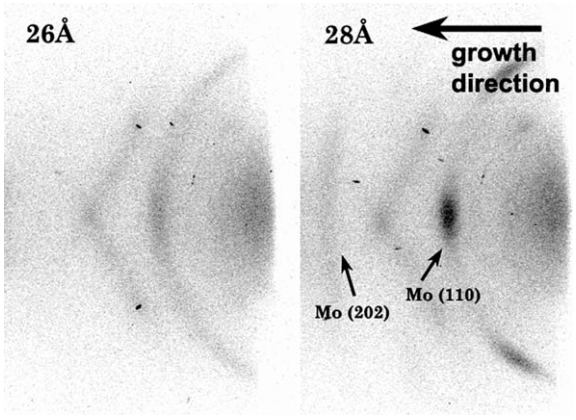

Fig. 4. X-ray micro-diffraction images for two periodic multilayers with Mo layer thickness just above (28 Å) and below (26 Å) the crystallisation threshold.

We can also see from the TEM cross-section view, the transition between amorphous to crystalline Mo has taken place for both bombardment energies, with an increase in thickness of a few angstroms. However the effective thickness of the layers is difficult to control and compare, because the net deposition rates are slightly different due to the resputtering effect with the higher ion energy. Therefore we can state that the critical Mo thickness above which the Mo layer starts to crystallize is about 2.6 nm. This value is really higher than that found in the standard Mo/Si system and is much closer to the Mo layer thickness values used in the mirror design for 13.5 nm reflectivity: this explains the amorphous structure that was sometimes found in $Mo/B_4C/Si/B_4C$ multilayer mirrors.

As reported for the Mo/Si multilayer case [9], the threshold thickness for Mo nano-crystal formation in our case is probably guided by the depth profile of impurities (Si, B and C) into the Mo layer: considering the blocking action exerted by the B_4C thin layer on the silicide formation and hence on the Mo–Si interdiffusion [26] and the considerably lower solubility limit of B in Mo (about 2 at.%) [27] compared to that of Si (about 7 at. %), we can assume that Mo nano-crystal formation will begin when the concentration of boron is below the solubility limit i.e. at a global Mo thickness higher than in the Mo/Si case without barrier layer. The presence of boron into the Mo lattice at the nm scale is difficult to measure. Indirect evidence can be given by the shift of the observed Mo(110) X-ray diffraction peak to

lower 2θ values measured in these layers (but not presented in this paper): this shift may be caused by stress [25] induced by the boron and carbon in the interstitial sites that cause an expansion of the lattice. This peak shift in XRD analysis and a change of first neighbours of Mo atoms in the presence of boron carbide or carbon interfaces by EXFAS analysis has already been observed and ascribed to the presence of boron and carbon atoms in the interstitial sites in the octahedral and tetrahedral positions [26]. On the other side the contribution to the stress of the Ar incorporation can be neglected, since in standard Mo/Si multilayers for similar layer thickness the diffraction shift does not appear, the lattice expansion is strictly correlated to the B_4C introduction.

To better quantify the Mo crystallization thickness, two periodic multilayer samples were produced with Mo thickness of 2.6 nm and 2.8 nm, respectively. Their thickness was controlled by RBS analysis and their crystal structure by μXRD image (Fig. 4). The X-ray patterns prove that one sample is above and the other below the crystallisation threshold, as it can be seen by the presence of the Mo(110) spot for the multilayer with thicker Mo layers. The spot appears in the same way as in the electron diffraction pattern in the direction that is normal to the sample surface. Furthermore we observe that the Mo nano-crystals start growing with a (110) preferential orientation. The grain size (as determined by the Scherrer equation) of the small crystals just above the transition region is very close to the Mo layer thickness.

4. Conclusions

We have shown that the introduction of thin B_4C barrier layers in the Mo/Si multilayers induces changes in Mo grain nucleation. In particular, the introduction of these thin barrier layers causes an increase in the Mo crystallisation thickness threshold relative to the results found in Mo/Si multilayers grown by sputtering without barrier layers. As in the case of Mo/Si multilayers, Mo crystal nucleation probably starts when boron concentration is lower than the solubility limit in Mo of 2 at.%; for higher concentrations of boron the crystal nucleation is hindered and an amorphous compound is produced. We suggest that the shift of the Mo(110) reflection found in XRD patterns, is due to the B incorporation into the Mo lattice. We can also observe that the ion energy in the energy window, which allows surface but not bulk diffusion, allows a decrease in the angular spread of the Mo(110) reflection along the growth direction, avoiding the formation of thick mixed interlayers.

Acknowledgements

This paper was prepared within the MIUR FIRB-RBNE01ABPB and INFN ARCHIMEDE projects.

References

[1] T.W. Barbee, EUV, X-ray and Gamma-Ray Instrumentation for Astronomy and Atomic Physics, vol. 1159, SPIE, 1989, p. 638.
[2] C.W. Gwyn, R. Stulen, D. Sweeney, et al., J. Vac. Sci. Technol., B 16 (1998) 3142.
[3] H. Takenaka, T. Kawamura, J. Electron Spectrosc. Relat. Phenom. 80 (1996) 381.
[4] T. Feigl, S. Yulin, T. Kuhlmann, et al., in: D.A. Tichenor, J.A. Folta (Eds.), Soft X-ray and EUV Imaging Systems II, vol. 4506, SPIE, San Diego, California, USA, 2001, p. 121.
[5] S. Bajt, J. Alameda, T. Barbee, et al., in: D.A. Tichenor, J.A. Folta (Eds.), Soft X-ray and EUV Imaging Systems II, vol. 4506, SPIE, San Diego, California, USA, 2001, p. 65.
[6] S. Braun, H. Mai, M. Moss, et al., Jpn. J. Appl. Phys. 41 (2002) 4074.
[7] M.B. Stearns, C.-H. Chang, D.G. Stearns, J. Appl. Phys. 71 (1992) 87.
[8] S. Bajt, J. Vac. Sci. Technol., A, Vac. Surf. Films 18 (2000) 557.
[9] S. Bajt, D.G. Stearns, P.A. Kearney, J. Appl. Phys. 90 (2001) 1017.
[10] V. Rigato, A. Patelli, X-ray and Inner-Shell Processes, vol. 652, AIP, Roma, Italy, 2002, p. 103.
[11] R. Liu, Z.S. Zheng, W.K. Chu, Nucl. Instrum. Methods B 108 (1996) 1.
[12] Y. Feng, Z. Zhou, Y. Zhou, et al., Nucl. Instrum. Methods B 86 (1994) 225.
[13] J. Liu, X. Lu, X. Wang, et al., Nucl. Instrum. Methods B 190 (2002) 107.
[14] N.J.M. Carvalho, J.T.M.D. Hosson, J. Mater. Res. 16 (2001) 2213.
[15] M.T. Robinson, J. Appl. Phys. 54 (1983) 2650.
[16] W. Eckstein, J.P. Biersack, Z. Phys., B 63 (1986) 471.
[17] J. Lindhard, M. Scharff, Phys. Rev. 124 (1961) 128.
[18] O. Oen, M.T. Robinson, Nucl. Instrum. Methods 132 (1976) 647.
[19] T.P. Drüsedau, M. Löhmann, B. Garke, J. Vac. Sci. Technol., A, Vac. Surf. Films 16 (1998) 2728.
[20] W. Eckstein, Computer Simulation of Ion-Solid Interactions, Springer, Berlin, 1991.
[21] R.E. Somekh, J. Vac. Sci. Technol., A, Vac. Surf. Films 2 (1984) 1285.
[22] Z.Q. Ma, Y. Kido, Thin Solid Films 359 (2000) 288.
[23] V. Rigato, A. Patelli, G. Maggioni, et al., Surf. Coat. Technol. 174–175 (2003) 40.
[24] L.G. Jacobsohn, R.D. Averitt, M. Nastasi, J. Vac. Sci. Technol., A, Vac. Surf. Films 21 (2003) 1639.
[25] A. Patelli, J. Ravagnan, V. Rigato, et al., Appl. Surf. Sci. 238 (2004) 262.
[26] T. Böttger, D.C. Meyer, P. Paufler, et al., Thin Solid Films 444 (2003) 165.
[27] H.F. McMurdie, A.E. McHale, H.M. Ondik, et al., Phase Diagrams for Ceramists, American Ceramic Society, Westerville, Ohio, 1964.